New Journal of Physics
The open access journal at the forefront of physics
Deutsche Physikalische Gesellschaft DPG | IOP Institute of Physics

# Structural phase transition associated with van Hove singularity in 5d transition metal compound $IrTe_2$

**T Qian[1], H Miao[1], Z J Wang[1], X Shi[1], Y B Huang[1], P Zhang[1], N Xu[1], L K Zeng[1], J Z Ma[1], P Richard[1,2], M Shi[3], G Xu[1], X Dai[1,2], Z Fang[1,2], A F Fang[1], N L Wang[1,2,4] and H Ding[1,2]**

[1] Beijing National Laboratory for Condensed Matter Physics, and Institute of Physics, Chinese Academy of Sciences, Beijing 100190, People's Republic of China
[2] Collaborative Innovation Center of Quantum Matter, Beijing, People's Republic of China
[3] Paul Scherrer Institute, Swiss Light Source, CH-5232 Villigen PSI, Switzerland
[4] International Center for Quantum Materials, School of Physics, Peking University, Beijing 100871, People's Republic of China
E-mail: tqian@iphy.ac.cn

Received 22 July 2014, revised 13 October 2014
Accepted for publication 5 November 2014
Published 15 December 2014

*New Journal of Physics* **16** (2014) 123038
doi:10.1088/1367-2630/16/12/123038

## Abstract

We have investigated the electronic states of $IrTe_2$ by using angle-resolved photoemission spectroscopy to elucidate the origin of the structural phase transition. Both the Ir 4f and Te 4d core level spectra exhibit dramatic splitting below the phase transition temperature $T_s$, suggesting that there exist two inequivalent Ir and Te sites with distinctly different electronic states in the distorted phase. The band related to the saddle points at the Fermi level ($E_F$) is strongly reconstructed, which removes the van Hove singularity from $E_F$ below $T_s$. The wavevector connecting the adjacent saddle points is consistent with the in-plane superstructure modulation wavevector. These results indicate that the phase transition in $IrTe_2$ is intimately associated with the saddle points. As the van Hove singularity mainly originates from the Te $p_x$+$p_y$ orbitals, the Te 5p electronic states play a dominant role in the structural phase transition.

Keywords: IrTe2, charge density wave, van Hove singularity

The proximity of superconductivity to other quantum ordered states is an important issue in condensed matter physics. Indeed, the interplay between them is believed to be closely related to the origin of superconductivity. For example, in cuprates, ferropnictides and ferrochalcogenides, and heavy fermion superconductors, the development of superconductivity is usually accompanied by a suppression in the long-range magnetic order. It is thus widely believed that the origin of their unconventional superconductivity in these materials is intimately associated with magnetic excitations, though the microscopic mechanisms are still a mystery [1–3]. Another typical example is the coexistence and competition between charge-density-wave (CDW) order and superconductivity in a number of compounds, which has also attracted much attention to their relationship [4–7].

Recently, the 5d transition metal dichalcogenide $IrTe_2$ with 1T-structure was suggested to be of the second case. $IrTe_2$ exhibits a structural phase transition from trigonal $P\bar{3}m1$ to triclinic $P1$ or $P\bar{1}$ at $T_s \sim 270$ K [8–10], below which a new structural modulation with a wavevector $Q = (1/5, 0, -1/5)$ was revealed [11]. With intercalation or substitution at the Ir sites of Pt, Pd, Rh or Cu, the structural transition is suppressed and bulk superconductivity is induced with $T_c$ up to ~3 K, indicating an interesting interplay between them [11–15]. Clarifying the origin of the structural transition is a crucial step to understanding the mechanism of the superconductivity. Yang *et al* proposed that the transition is driven by partial Fermi surface (FS) nesting, and therefore of a CDW-type through the involvement of the Ir 5d orbitials [11]. However, no energy gap, characteristic of a density-wave type transition, was identified from the optical conductivity spectra [12]. Several other mechanisms, including the orbital-induced Peierls instability [16, 17], the reduction of kinetic energy by crystal field effects [12], interlayer hybridization [14], local bonding instability [8], depolymerization–polymerization of Te bonds [18], and Ir dimerization [9, 10], have been proposed to understand the structural transition.

In this work, we reveal that the phase transition in $IrTe_2$ is intimately associated with the van Hove singularity (vHs) at the Fermi level ($E_F$). The vHs arises from the saddle points around the Brillouin zone boundary and the wavevector between the adjacent saddle points is $q \sim (1/5, 0, 0)$, which is consistent with the in-plane structural modulation wavevector. The band related to the saddle points is dramatically reconstructed below $T_s$, leading to a significant reduction of the electronic energy, which is likely to be the driving force for the transition.

High quality single crystals of $IrTe_2$ were grown via the self-flux technique [12]. Angle-resolved photoemission spectroscopy (ARPES) experiments were performed at beamline PGM of the Synchrotron Radiation Center (Wisconsin), at beamline 4.0.3.2 of the Advanced Light Source (California), and beamline SIS of the Swiss Light Source (Switzerland) with Scienta R4000 analysers. The energy and angular resolutions were set at 30 meV and 0.2°, respectively. For the ARPES measurements, the samples were cleaved *in situ* and measured in a vacuum better than $3 \times 10^{-11}$ Torr. Calculations for the electronic structure and density of states (DOS) were performed by using the full-potential augmented plane-wave and Perdew–Burke–Ernzerhof parameterization of the generalized gradient approximation (GGA–PBE) exchange-correlation function [19] as implemented in the WIEN2 k code [20]. The spin–orbit interactions were included by using a second variational procedure. The muffin-tin radii ($R_{MT}$) were set to 2.50 Bohrs for Ir and 2.26 Bohrs for Te. The plane-wave cutoff ($K_{max}$) was determined by $R_{min}K_{max} = 7.0$, where $R_{min}$ is the minimal $R_{MT}$.

We start with the Te 4d and Ir 4f core level photoemission spectra, which can yield valuable information on the valence and chemical environment of the constituent elements.

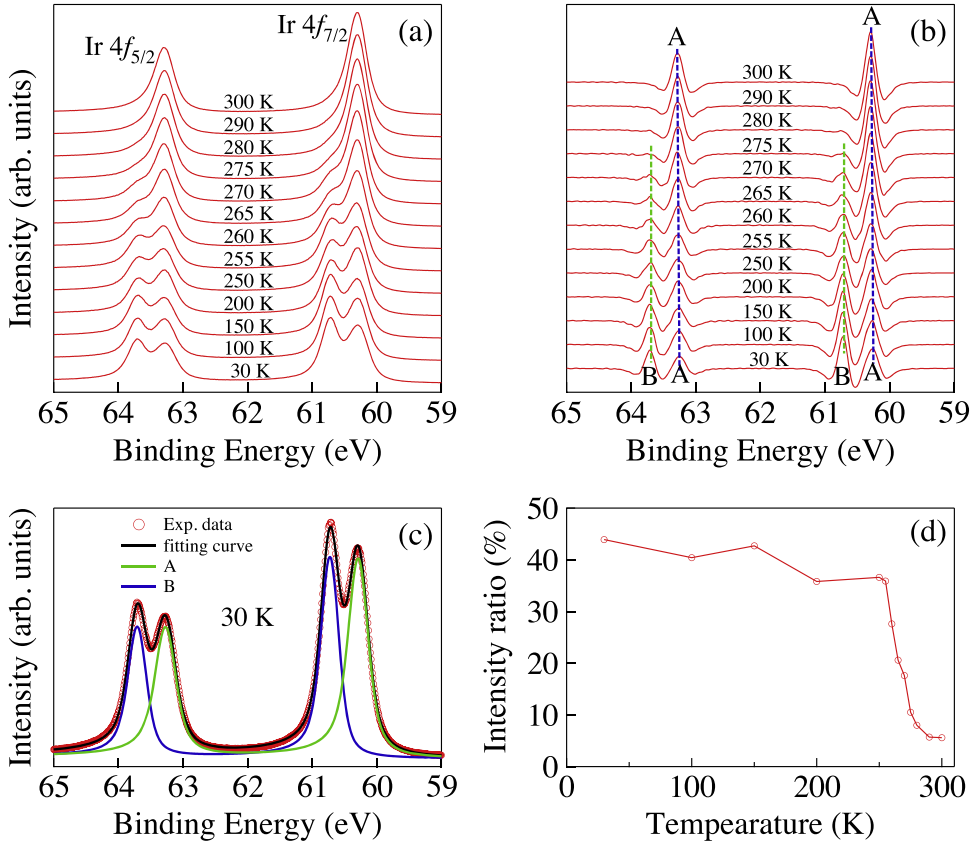


**Figure 1.** (a) Photoemission spectra of the Ir 4f core lines taken with $h\nu = 140$ eV at various temperatures. (b) Second derivatives of the spectra shown in panel (a). Dashed lines are guides for eyes to trace the peak positions. (c) Ir 4f photoemission spectrum taken at 30 K with fitted curves. The spectrum is fitted to two sets of peaks with Doniach–Sunjic line shape convoluted by a Gaussian with FWHM of 0.26 eV. (d) Ratio of the area of peaks *B* to the total area as a function of temperature.

While a previous study has shown no change in the Te 3d peaks and a slight increase in the Ir 4f peak width at low temperature [17], our high-resolution measurements reveal clear splitting of the Ir 4f and Te 4d peaks below $T_s$.

Figures 1(a) and (b) show the Ir 4f core level spectra and their second derivatives at various temperatures, respectively. A set of peaks (labeled as *A* in figure 1(b)) induced by the spin–orbit coupling is observed above $T_s$. The binding energy ($E_B$) of Ir $4f_{7/2}$ in $IrTe_2$ is 60.3 eV at 300 K, which is obviously lower than in $IrO_2$ (62.0 eV, $Ir^{4+}$) [21] and $CuIr_2S_4$ (~61.0 eV, $Ir^{3.5+}$) [22]. This suggests that the valence of Ir in $IrTe_2$ is less than +3.5 in the high temperature phase. Our results are also consistent with the structure data, where the average Te–Te bond length $d_{Te-Te}$= 3.528 Å in $IrTe_2$ is noticeably shorter than the usual value of 4.03 Å of regular $Te^{2-}$ in classic $CdI_2$-like arrangement (e.g. $HfTe_2$), making the valence state of Te close to −1.5 [23].

Upon cooling below $T_s$, a new set of peaks (*B*) develops on the higher $E_B$ side of *A* in figures 1(a) and (b). The energy difference $\Delta_{AB}$ between *A* and *B* depends slightly on temperature and is ~0.44 eV at 30 K. The development of peaks *B* suggests that the electronic states of partial Ir atoms are changed across the phase transition while the other Ir atoms

associated with the peaks *A* below $T_s$ are not essentially affected. The results are consistent with the recently reported structural data [9, 10], which reveal that two of five Ir atoms per unit cell form the Ir–Ir dimer in the distorted phase. The 5d orbital occupancy for the two dimerized Ir atoms is reduced whereas the occupancy for the other three Ir atoms is little affected. The spectra below $T_s$ are fitted to two sets of peaks with the Doniach–Sunjic line shape in figure 1(c). The ratio of the area of peaks *B* to the total area as a function of temperature is plotted in figure 1(d). The intensity ratio is at ∼40% below 250 K, further confirming that the peaks *B* are associated with the dimerized Ir atoms.

Similar splitting is also observed in the Te 4d core level spectra below $T_s$, as shown in figure 2, indicating that charge disproportion occurs on both the Ir and Te sites. Two sets of peaks of Te 4d (*C* and *D*) are identified above $T_s$. A possible reason for the double-peak feature is that they may originate from two different screening channels, where the screening charge comes from the Te 5p conduction bands and the Ir 5d ligand orbitals, respectively. Similar double-peak features have been also observed in $La_{1-x}Sr_xMnO_3$ and $V_2O_3$, and interpreted in the same way [24, 25]. Another possibility is surface effect. As the cleavage occurs between two adjacent Te plane, the terminal layer is constituted with the Te atoms that may have valence and chemical environments different from those in the bulk. Upon cooling below $T_s$, four sets of peaks (*E*, *F*, *G*, and *H*) are identified. The spectra above and below $T_s$ are fitted to two and four sets of peaks with the Doniach–Sunjic line shape, respectively. The peak positions determined by fitting are plotted as a function of temperature in figure 2(e). The energy differences $\Delta_{EG}$ and $\Delta_{FH}$ are equal for all temperatures below $T_s$ and are ∼0.46 eV at 30 K. Note that upon cooling below $T_s$, the Ir 4f spectra show a broad change while the Te 4d spectra do a first-order like change. These different behaviors are most likely related to the dominant role of the Te 5p electronic states in the structural phase transition as discussed below. Moreover, the original Te 4d peaks (*C* and *D*) are completely replaced below $T_s$, indicating that the electronic states of all the Te atoms are reconstructed across the phase transition. The changes in the Ir 4f and Te 4d core level peaks suggest that there exist two inequivalent Ir and Te sites with different electronic states in the distorted phase.

In figure 3 we show the changes of the low-energy electronic structure across the phase transition. Figures 3(a) and (b) show the FS intensity maps with photon energy $h\nu$ = 90 eV (corresponding to the $k_z \sim 0.8\pi$ plane) measured at 300 and 30 K, respectively. We observe one outer and three inner hole-like FS pockets at 300 K, in agreement with the calculated ones at $k_z = 0.8\pi$ for the high-temperature trigonal phase. According to their calculations, Yang *et al* proposed a FS nesting between one of the corners of the outer pocket at $k_z = 0.8\pi$ and the inner pocket at $k_z = 0.4\pi$ with a wavevector of (1/5, 0, −1/5) [11]. To inspect whether there exists any energy gap induced by this nesting, we show in figures 3(d) and (e) the ARPES spectra along the $k_x = -0.55$ Å$^{-1}$ cut at 300 and 30 K, respectively. The spectra exhibit a clear Fermi edge at 30 K, suggesting that no CDW-type gap is induced in the proposed nesting FS section.

The most prominent change in the low temperature phase is that the three inner pockets disappear at 30 K. To clarify this, we compare in figures 3(f)–(i) the band dispersions along the $k_x = -0.35$ Å$^{-1}$ cut at 300 and 30 K. While the inner hole-like band crosses $E_F$ at 300 K, forming the inner FS pocket, it sinks below $E_F$ at 30 K, leading to a large energy gap of ∼0.3 eV. From the intensity map at $E_B = 0.3$ eV and 30 K in figure 3(c), we observe again three highlighted areas, corresponding to the band tops, whose momentum locations are consistent with those of the inner FS pockets at 300 K. This indicates that the change in the FS topology arises from an energy shift of the related band. According to the band calculations, the near-$E_F$ band that forms

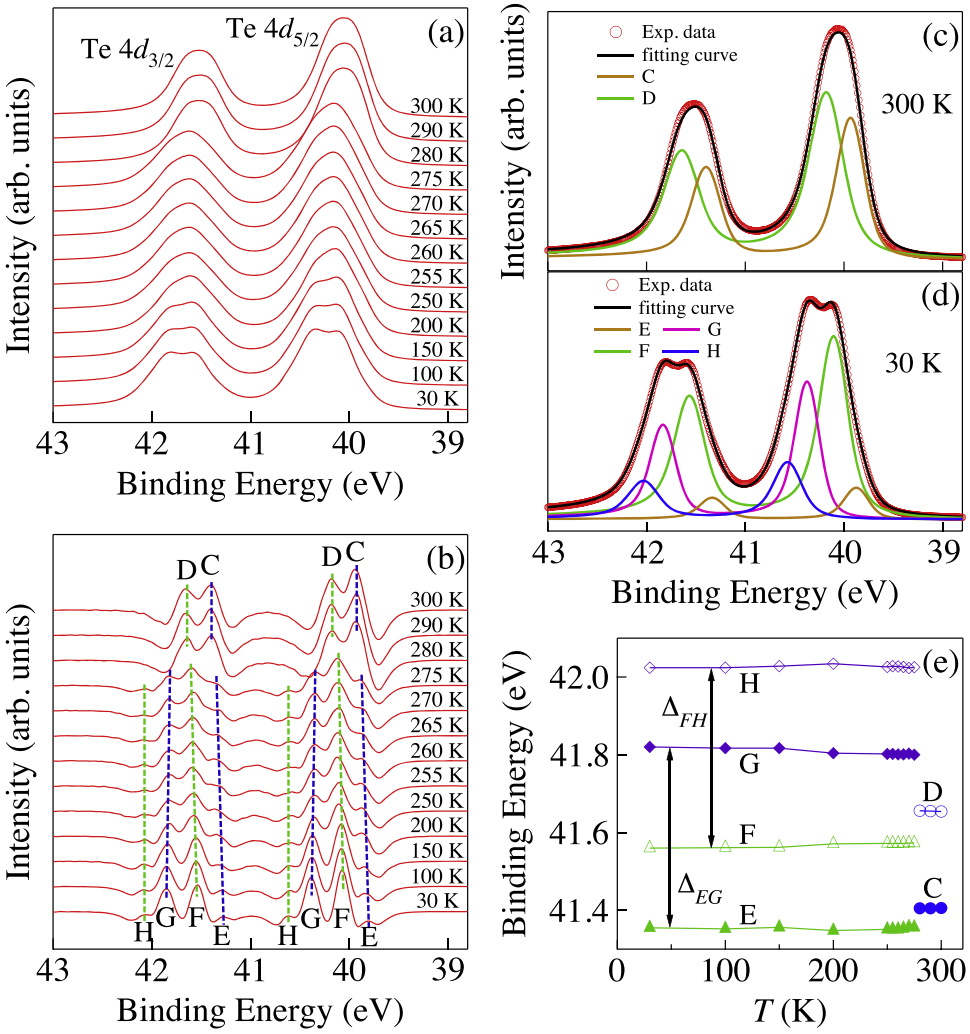


**Figure 2.** (a) Photoemission spectra of the Te 4d core lines taken with $h\nu = 90$ eV at various temperatures. (b) Second derivatives of the spectra shown in panel (a). Dashed lines are guides for eyes to trace the peak positions. (c) and (d) Te 4d photoemission spectra taken at 300 and 30 K with fitted curves, respectively. The spectra at 300 and 30 K are fitted to two and four sets of peaks with the Doniach–Sunjic line shape convoluted by a Gaussian with FWHM of 0.26 eV, respectively. (e) Energy positions of maxima of the *C*, *D*, *E*, *F*, *G* and *H* peaks for the Te $4d_{3/2}$states, determined from the fitted curves as exemplified in panels (c) and (d), as a function of temperature. $\Delta_{EG}$ ($\Delta_{FH}$) represents the energy difference between the peaks *E* and *G* (*F* and *H*).

the inner pockets originates mainly from the Te $p_x$+$p_y$ orbitals. As seen in figure 4(b), the partial DOS from the Te $p_x$+$p_y$ orbitals exhibits a distinct peak located very close to $E_F$. The large energy shift of the Te $p_x$+$p_y$ band reduces the DOS at $E_F$ significantly and thus lowers the electronic energy. This is likely to be the driving force for the transition.

We further find that the distinct peak in the DOS is a van Hove singularity. According to the calculated band structure in figure 4(d), on moving from the *A* point to the *L* and *H* points, the Te $p_x$+$p_y$ band disperses first towards $E_F$ and then to higher $E_B$, leading to band tops at $k_{//}$ ~0.36 Å$^{-1}$ indicated by arrows. This band crosses and sinks below $E_F$ along *AH* and *AL*,

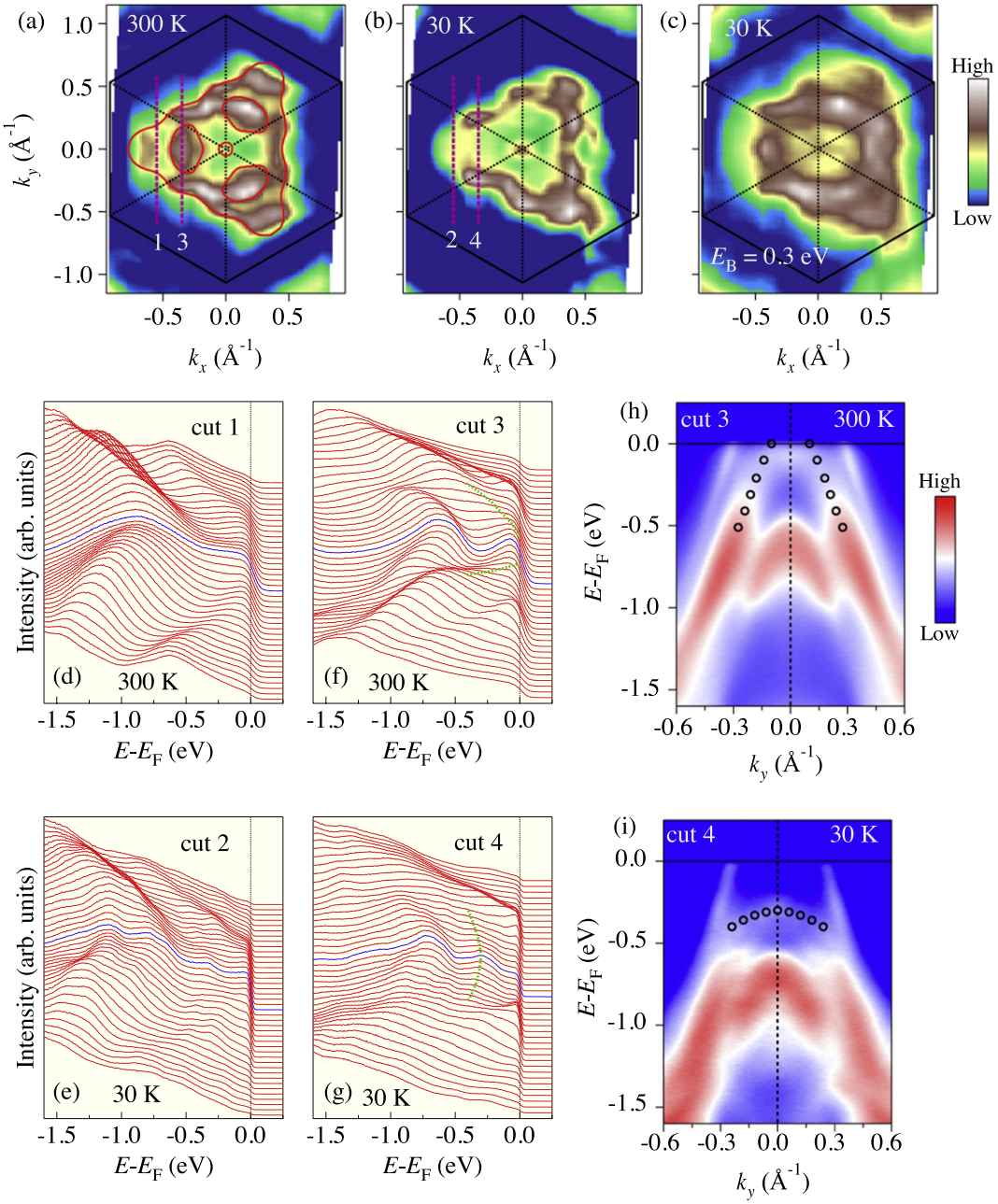


**Figure 3.** (a) ARPES intensity plot at $E_F$ taken with $h\nu = 90$ eV at 300 K, corresponding to $k_z \sim 0.8\pi$. The intensity is obtained by integrating the spectra within ± 10 meV with respect to $E_F$. The calculated FSs at $k_z = 0.8\pi$ for the trigonal phase are plotted for comparison. (b) Same as (a) but taken at 30 K. (c) Same as (b) but integrated with respect to $E_B = 0.3$ eV. (d) and (e) ARPES spectra recorded along cuts 1 and 2 at $k_x = -0.55$ Å$^{-1}$ from panels (a) and (b), respectively. (f) and (g) ARPES spectra recorded along cuts 3 and 4 at $k_x = -0.35$ Å$^{-1}$ from panels (a) and (b), respectively. Green dashed lines are guides for eyes to trace the band dispersions. Blue curves indicate the spectra at $k_y = 0$. (h) and (i) ARPES intensity plots along cuts 3 and 4, respectively. Open circles are guides for eyes to trace the band dispersions.

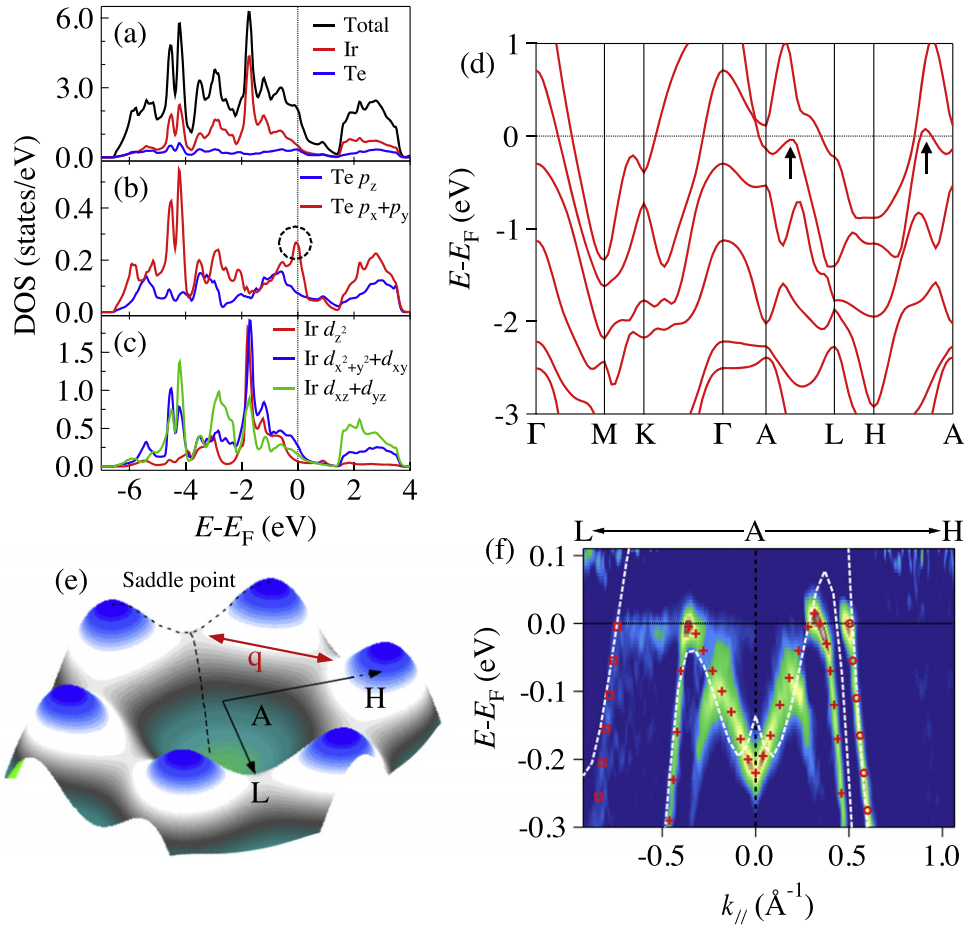


**Figure 4.** (a) Total and partial DOS from the Te 5p and Ir 5d states. (b) Partial DOS from different Te 5p orbitals. (c) Partial DOS from different Ir 5d orbitals. (d) Calculated band structure for the trigonal phase. The arrows indicate the tops of the band from the Te $p_x$+$p_y$ orbitals along *AL* and *AH*. (e) Three-dimensional representation around the saddle points at $k_z = \pi$. The red arrow indicates the momentum transfer connecting the adjacent saddle points. (f) Intensity plot of the two-dimension curvature [28] along *L*–*A*–*H* taken with $h\nu = 96$ eV at 300 K. Red symbols are guides for eyes to trace the band dispersions. White dashed curves represent the calculated bands. The hole-like band that is not predicted by the calculation is from the zone near $k_z = 0$ due to the short photoelectron mean free path perpendicular to the surface.

respectively, forming six small hole pockets at $k_z = \pi$ [16, 26, 27]. In figure 4(e), one can identify six saddle points located along the *AL* lines, at which the band dispersions are hole- and electron-like along and perpendicular to *AL*, respectively. It is worth noting that the momentum transfer $q$ connecting the adjacent saddle points is ∼(1/5, 0, 0), which is consistent with the in-plane projection of the structural modulation wavevector $Q = (1/5, 0, -1/5)$. In figure 4(f), we compare the experimental band dispersions and the calculated ones along *L*–*A*–*H*. The excellent consistency in the experimental and calculated data supports the scenario of the saddle points, whose energy position in experiment is just located at $E_F$.

Our results indicate that the structural transition in $IrTe_2$ is intimately associated with the vHs at $E_F$. Firstly, the band near the saddle points is strongly reconstructed, which removes the

vHs from $E_F$ and thus lowers the electronic energy. Secondly, the wavevector between the adjacent saddle points is consistent with the in-plane structural modulation wavevector. This is reminiscent of the Rice–Scott 'saddle-point' mechanism [5, 29, 30]. In this model, the susceptibility diverges logarithmically at a wavevector connecting two saddle points, leading to a CDW instability, and the FS is truncated near the saddle points, which seems to be in agreement with our observation in $IrTe_2$. The energy scale of the electronic structure change near the saddle points is very large compared to the expectation from the BCS mean-field theory for a CDW transition, which is most likely due to strong fluctuation effects as suggested in some other low-dimensional density wave materials [31–33].

In the scenario of vHs, the structural phase transition can be associated with a giant Kohn anomaly induced by the scattering of conduction electrons between the adjacent saddle points. To examine this point, it is desirable to perform inelastic x-ray or neutron scattering measurements of phonon dispersions as the existence of a soft phonon mode at a specific momentum is the direct evidence of a CDW transition. Within this picture, the stripe-like 1/5 superstructure in the *a*–*b* plane as observed in the high-resolution transmission electron microscope [18] and scanning tunneling microscopy [35] images is a direct consequence of the scattering between the adjacent saddle points with strong coupling of charge and lattice degrees of freedom. Since the adjacent $IrTe_2$ layers are coupled via the Te–Te bonds pointing to the (1, 0, −1) direction, the in-plane superstructure naturally leads to the superstructure modulation with $Q = (1/5, 0, -1/5)$ in three-dimension.

In the general vHs scenario, various states, including CDW, spin-density-wave, phase separation, and even superconductivity, may be induced to remove the singularity from $E_F$ and lower the electronic energy. One interesting question is whether superconductivity is also driven by the vHs since the opening of a superconducting gap in the vicinity of the saddle points could remove the vHs from $E_F$. As the phase diagrams of doping and pressure exhibit a seemingly competitive interplay between superconductivity and other ordered phases [11–15, 35], our present study, which reveals the vHs origin of the phase transition in $IrTe_2$, should motivate further experimental and theoretical studies on the relationship between superconductivity and adjacent quantum ordered states.

## Acknowledgments

We acknowledge W Ku, T Xiang, ZY Lu, GL Cao, HF Tian, JQ Li, XD Zhou, and YY Wang for valuable discussions. This work was supported by grants from MOST (2010CB923000, 2013CB921700, 2011CBA001000, 2011CB921701 and 2012CB821403), CAS (2010Y1JB6 and XDB07000000), NSFC (11004232, 11050110422, 11204359, 11120101003, 11074291, 11121063, 11234014, and 11274362), and SSSTC (IZLCZ2 138954). This work is based in part on research conducted at the Synchrotron Radiation Center, which is primarily funded by the University of Wisconsin-Madison with supplemental support from facility users and the University of Wisconsin-Milwaukee. This work is based in part upon research conducted at the Swiss Light Source, Paul Scherrer Institute, Villigen, Switzerland. The Advanced Light Source is supported by the U.S. Department of Energy, Office of Science, Office of Basic Energy Sciences, under contract no. DE-AC02-05CH112.

## References


[1] Mook H A, Dai P C, Hayden S M, Aeppli G, Perring T G and Dogan F 1998 *Nature* **395** 580
[2] Christianson A D *et al* 2008 *Nature* **456** 930
[3] Mathur N D, Grosche F M, Julian S R, Walker I R, Freye D M, Haselwimmer R K W and Lonzarich G G 1998 *Nature* **394** 39
[4] Morosan E, Zandbergen H W, Dennis B S, Bos J W G, Onose Y, Klimczuk T, Ramirez A P, Ong N P and Cava R J 2006 *Nat. Phys.* **2** 544
[5] Kiss T, Yokoya T, Chainani A, Shin S, Hanaguri T, Nohara M and Takagi H 2007 *Nat. Phys.* **3** 720
[6] Borisenko S V *et al* 2009 *Phys. Rev. Lett.* **102** 166402
[7] Zhao J F *et al* 2007 *Phys. Rev. Lett.* **99** 146401
[8] Cao H B, Chakoumakos B C, Chen X, Yan J Q, McGuire M A, Yang H, Custelcean R, Zhou H D, Singh D J and Mandrus D 2013 *Phys. Rev.* B **88** 115122
[9] Pascut G L, Haule K, Gutmann M J, Barnett S A, Bombardi A, Artyukhin S, Vanderbilt D, Yang J J, Cheong S W and Kiryukhin V 2014 *Phys. Rev. Lett.* **112** 086402
[10] Toriyama T, Kobori M, Konishi T, Ohta Y, Sugimoto K, Kim J, Fujiwara A, Pyon S, Kudo K and Nohara M 2014 *J. Phys. Soc. Japan* **83** 033701
[11] Yang J J, Choi Y J, Oh Y S, Hogan A, Horibe Y, Kim K, Min B I and Cheong S W 2012 *Phys. Rev. Lett.* **108** 116402
[12] Fang A F, Xu G, Dong T, Zheng P and Wang N L 2013 *Sci. Rep.* **3** 1153
[13] Pyon S, Kudo K and Nohara M 2012 *J. Phys. Soc. Japan* **81** 053701
[14] Kamitani M, Bahramy M S, Arita R, Seki S, Arima T, Tokura Y and Ishiwata S 2013 *Phys. Rev.* B **87** 180501
[15] Kudo K, Kobayashi M, Pyon S and Nohara M 2013 *J. Phys. Soc. Japan* **82** 085001
[16] Ootsuki D *et al* 2013 *J. Phys. Soc. Japan* **82** 093704
[17] Ootsuki D *et al* 2012 *Phys. Rev.* B **86** 014519
[18] Oh Y S, Yang J J, Horibe Y and Cheong S W 2013 *Phys. Rev. Lett.* **110** 127209
[19] Perdew J P, Burke K and Ernzerhof M 1996 *Phys. Rev. Lett.* **77** 3865
[20] Blaha P, Schwarz K, Madsen G, Kvasnicka D and Luitz J WIEN2 K package available at http://www.wien2k.at.
[21] Chung W H, Wang C C, Tsai D S, Jiang J C, Cheng Y C, Fan L J, Yang Y W and Huang Y S 2010 *Surf. Sci.* **604** 118
[22] Okane T *et al* 2004 *J. Magn. Magn. Mater.* **272–276** e297–8
[23] Jobic S, Deniard P, Brec R, Rouxel J, Jouanneaux A and Fitch A N 1991 *Z. Anorg. Allg. Chem.* **598** 199
[24] Horiba K *et al* 2004 *Phys. Rev. Lett.* **93** 236401
[25] Kamakura N *et al* 2004 *Europhys. Lett.* **68** 557
[26] Ootsuki D *et al* 2014 *J. Phys. Soc. Japan* **83** 033704
[27] Yu D J *et al* 2014 *Phys. Rev.* B **89** 100501(R)
[28] Zhang P, Richard P, Qian T, Xu Y M, Dai X and Ding H 2011 *Rev. Sci. Instrum.* **82** 043712
[29] Rice T M and Scott G K 1975 *Phys. Rev. Lett.* **35** 120
[30] Liu R, Tonjes W C, Greanya V A, Olson C G and Frindt R F 2000 *Phys. Rev.* B **61** 5212
[31] Dressel M and Grüner G 2002 *Electrodynamics of Solids: Optical Properties of Electrons in Matter* (Cambridge: Cambridge University Press)
[32] Huang Y, Wang H P, Wang W D, Shi Y G and Wang N L 2013 *Phys. Rev.* B **87** 100507
[33] Huang Y, Wang H P, Chen R Y, Zhang X, Zheng P, Shi Y G and Wang N L 2000 *Phys. Rev.* B **89** 155120
[34] Machida T, Fujisawa Y, Igarashi K, Kaneko A, Ooi S, Mochiku T, Tachiki M, Komori K, Hirata K and Sakata H 2013 *Phys. Rev.* B **88** 245125
[35] Kiswandhi A, Brooks J S, Cao H B, Yan J Q, Mandrus D, Jiang Z and Zhou H D 2013 *Phys. Rev.* B **87** 121107